RESEARCH ARTICLE

European Journal of
Lipid Science and Technology
www.ejlst.com

Characterization of Oleogels Based on Waxes and Their Hydrolyzates

Till Wettlaufer, Birgit Hetzer, and Eckhard Flöter*

In this paper, the structuring of liquid oils, also known as oleogelation, is systematically investigated for the first time using a quasi-quaternary mixing system approach. Native waxes with different quantities of wax esters (WE), *n*-alkanes (hydrocarbons (HC)), fatty acids (FA), and fatty alcohols (FaOH) are applied in mixtures with hydrolyzed waxes to systematically change the composition. Hydrolyzed waxes contain high levels of FA and FaOH. The model systems are investigated on microscopic level (brightfield light microscopy (BFM), cryogenic scanning electron microscopy (cryo-SEM)) as well as on their macroscopic properties (rheology, gel hardness) and calorimetric behavior (differential scanning calorimetry (DSC)). It is found that sunflower wax (SFW)-based gels (12% structurant) become less hard on any admixture. Beeswax (BW)-based gels show significant increases in hardness when 25% and 50% (w/w) hydrolyzate are admixed. This could be related to stepwise crystallization. Further analysis reveals that the dissolution/melting behavior of the wax ester mixtures can be surprisingly well described as ideal solubility of a single pseudocomponent. The approach to unravel the individual contributions of the different species present in waxes is successful and marks a first step to better understand the systematic of wax functionality as oleogelators.

***Practical Application*: The substitution of hardstock fats in structured oil phases is of interest for two reasons. The improved nutritional profile oleogels offer are beneficial for public health while the elimination of palm oil based ingredients appears to be a general public desire. Among the technical solutions for non-TAG oil structuring waxes are very promising. This is primarily due to their availability, prior consumption, potentially low cost for functionality. Currently waxes are technically and scientifically wrongly treated as single components. In order to better utilize the potential of waxes and design future sourcing strategies it is necessary to understand the wax functionality at a compositional/molecular level. This contribution marks the first step into this direction by considering classes of molecules with respect to their contribution to functionality. This understanding is considered as a key for future compositional design.**

1. Introduction

In many food products, triacylglyceride-structured fat phases are related to desired product characteristics and processing properties. Unfortunately, so-called hardstock fats have intrinsically high levels of saturated fatty acids, or if generated via partial hydrogenation, today unacceptably high amounts of trans-fatty acids. The negative health effects of trans-fatty acids are evident since they increase the risk of coronary heart diseases and decrease serum high-density lipoprotein cholesterol (HDL).[1] Monounsaturated (MUFA) and polyunsaturated fatty acids (PUFA), which naturally occur in plant-based oils, are proven to lower the LDL and increase the HDL values. Unfortunately, the necessary physical characteristics hardstock fats supply to lipid phases is crucial for a wide range of product applications.[2,3] Triacylglycerides (TAG) composed of predominantly unsaturated fatty acids cannot deliver this necessary structure. The gelation of liquid oils is a potential technique to establish the physical properties needed. The so-called oleogelation/organogelation uses non-TAG structuring agents to immobilize the liquid oil in a 3D lattice. This results in a structured lipid phase with a semi-solid character. Among various structuring agents, waxes appear to be most promising, since they structure – without any prior chemical modification – liquid oils at low inclusion levels (0.3–4% w/w).[4–6] It is furthermore beneficial that waxes can source from numerous plant or animal origins and have a record of previous consumption. Waxes frequently considered for oil structuring

DOI: 10.1002/ejlt.202000345

T. Wettlaufer, Prof. E. Flöter
Department of Food Process Engineering
Technische Universität
Seestraße 13, Berlin, Berlin 13353, Germany
E-mail: till.wettlaufer@tu-berlin.de

Dr. B. Hetzer
Department of Food Technology and Bioprocess Engineering
Max Rubner-Institut
Karlsruhe 76131, Germany

European Journal of Lipid Science and Technology
www.ejlst.com

purposes are sunflower wax (SFW),[7,8] rice bran wax (RBW),[9–11] candelilla wax (CLW),[12,13] carnauba wax,[14,15] and beeswax (BW).[16] Although some attempts have been made to characterize wax-based oleogels in general, the related knowledge base remains highly fragmented. This is due to the lack of comparability of different studies due to variations of internal factors, such as concentration, composition, and type of wax, oil type and quality (mainly polar minor components)[17] and external factors, e.g., cooling rate, shear, storage conditions.[18] A useful effort to elucidated the effect of shear and cooling rate on the crystallization behavior of different waxes was reported by Blake and Marangoni.[4,19] However, some characteristics of wax oleogels such as the high melting temperatures, possible brittleness, and large crystal sizes, lengths larger 30 µm, result in unfavorable sensory characteristics. High melting temperatures have been reported to yield a waxy mouthfeel by covering of the oral cavity. To address this issue, different options have already been explored. The primary target is the dissolution characteristics and thus a reduction of the gel-sol transition temperature through additional components by either mixed crystal formation or crystal habit modification. Promising components to add are other waxes, emulsifiers or even high melting triacylglycerols. Pérez-Monterroza, Ezequiel J., Márquez-Cardozo, Carlos J., Ciro-Velásquez, J. Héctor combined BW with mono/diglycerides and SPAN 60 (sorbitan monostearate) and found, that the mixtures with SPAN 60 showed delayed crystallization onset and smaller wax crystals.[20] M. Chopin-Doroteo, J.A. Morales-Rueda, E. Dibildox-Alvarado, M. A. Charó-Alonso, A. La Peña-Gil, J. F. Toro-Vazquez combined candelilla wax with tripalmitin and claimed positive effects for the solid lipid contentand the gel's elasticity.[21]

In particular, combinations of different waxes appear to be a promising route to manipulate the properties of wax-based oleogels. The manipulation of oleogel properties was studied for combinations of SFW, RBW – both high melting – and Berry wax (BEW) (low melting).[11] Increased sample hardnesses found were explained by sintering due to sequential crystallization. Also, J. K. Winkler-Moser, J. Anderson, F. C. Felker, H.-S. Hwang evaluated binary wax mixtures, BW:CLW, BW:SFW, and SFW:CLW, as structuring system.[16] This study confirms that mixing of waxes can result in "excess hardness". Unfortunately, none of these studies includes an attempt to map the gel characteristics against the molecular composition of the different structuring systems. Currently one finds numerous other publications relating wax-based oleogels that do not report the molecular compositions. Waxes contain, dependent on their source, different types of esters, varying levels of fatty acids and fatty alcohols, hydrocarbons, and mixtures thereof. Regardless, there are some studies on the ability of possible subsystems of waxes to gel oil. For example, oleogelation by combinations of fatty acids and fatty alcohols has been reported.[22–25]

No systematic study to relate the molecular composition of the wax-based structuring systems to functionality has been reported yet. This leaves the attempt to design mixed wax structuring systems an endeavor with coincidental success. The authors belief that to overcome this shortcoming and allow for an a priori prediction of the performance of waxes and wax mixtures, it is necessary to elucidate the respective effect of the different components in waxes on oleogelation. To establish such a functional relation is cumbersome and hampered by the lack of availability of pure components, but it would allow to design oleogels taking product constraints such as disintegration temperature, hardness, shear sensitivity and alike into account.

To this end, this manuscript tries to make a first step by mapping the functionality of structuring systems made up of waxes and hydrolyzed waxes. Even though the mixtures based sunflower wax and beeswax and their respective hydrolyzates do not represent compositional changes at molecular level, changes are very systematic when mixing a wax with its hydrolyzate.

Table 1. Fatty acid composition (% area) of canola oil based on gas chromatographic FAME-determination.

Fatty acid	Chain length	Frequency [%]
Palmitic acid	16:0	4.4 ± 0.07
Palmitoleic acid	16:1	0.2 ± 0.01
Stearic acid	18:0	1.6 ± 0.01
Oleic acid	18:1	64.2 ± 0.19
Linoleic acid	18:2	18.6 ± 0.11
Linolenic acid	18:3	8.2 ± 0.25
Arachidic acid	20:0	0.6 ± 0.05
Eicosenoic acid	20:1	1.3 ± 0.05
Behenic acid	22:0	0.3 ± 0.01
Erucic acid	22:1	0.2 ± 0.08
Lignoceric acid	24:0	0.1 ± 0.01
Nervonic acid	24:1	0.1 ± 0.01

2. Experimental Section

2.1. Materials

Canola oil (refined) was contributed by Gustav Heess GmbH (Leonberg, Germany). Polarity of the oil (4.6% total polar compounds) was determined by Testo 270 cooking oil tester (Testo, Titisee-Neustadt, Germany). The fatty acid composition is given in **Table 1** (According to DFG method C-VI 10a). Sunflower wax (6607L, Lot.nr. F1911020-001) (SFW), beeswax (8108LM, Lot.nr. F1727017-001) (BW), sunflower wax-hydrolyzate (6607H, Lot.nr. F1637034-001) (SFWh) and beeswax-hydrolyzate (CERA H, Lot.nr. F1746044-001) (BWh) were kindly supplied by Kahlwax GmbH & Co KG (Trittau, Germany). All materials were used without further modification or purification.

2.1.1. Composition of Waxes

Wax is a naturally occurring material, originating from animal and plant sources. Based on extraction and purification processes, the composition fluctuates. Nevertheless, waxes exhibit distinct characteristics per respective source. C. D. Doan, C. M. To, M. Vrieze, F. Lynen, S. Danthine, A. Brown, K. Dewettinck, A. R. Patel. examined the composition of different waxes using HPLC-ELSD and GC-MS methods.[26] The composition of the hydrolyzed wax esters is based on the data of the original wax combined with the specification given by the supplier, 20% (w/w) of original wax esters present after hydrolyzation (Kahlwax, private

European Journal of Lipid Science and Technology
www.ejlst.com

Table 2. Typical composition of sunflower wax (SFW), beeswax (BW), and their corresponding hydrolyzates (Doan et al.[26], Kahlwax, private correspondence, hydrolyzed waxes calculated assuming random hydrolyzation). Data are normalized on reported major components.

	SFW	BW	SFWh	BWh
n-Alkane (% w/w)	0.2	26.9	0.2	26.9
WE (% w/w)	96.2	58.0	20.0[a)]	20.0[a)]
FA (% w/w)	3.3	8.8	41.4	27.8
FaOH (% w/w)	0.3	6.4	38.4	25.4

[a)] Supplier information.

communication). Furthermore, it was assumed that hydrolyzation was unspecific such that the composition in terms of fatty acid moieties (FA) and fatty alcohols moieties (FaOH) was identical in the ester and hydrolyzate fractions. Fractions in **Table 2** are normalized to 100%.

Beyond the primary characteristics displayed in Table 2, more detail of the wax composition are available.[26] The wax esters are the main component in SFW (96.2% w/w) covering primarily chain lengths of C44 to C50. The main fatty acid was C20:0. The main fatty alcohol was C24:0-OH. The 58% (w/w) wax esters in BW (C40 to C48) comprise shorter fatty acids, mainly C16:0, and longer fatty alcohols, C24-OH to C30-OH, than SFW. The significant portion of alkanes in BW (27%) was composed of hydrocarbon chains with up to 33 carbon atoms. The amounts of free fatty acids and free fatty alcohols of 8.8% and 6.4% (w/w) indicate a different carbon number make up than the BW wax esters, making it unlikely that these were simply resulting from hydrolysis of original esters.

2.2. Methods

2.2.1. Preparation of Oleogels

Oleogels based on canola oil and different wax-based structuring systems were prepared. The four different structuring systems were composed by combination of waxes and hydrolyzed waxes. For all systems, SFW:SFWh, SFW:BWh, BW:SFWh, and BW:BWh, mixing ratios of 0:100, 25:75, 50:50, 75:25, and 100:0 were studied at 12% and 8% (w/w) concentration of the structuring system in canola oil. These inclusion levels were established in preliminary experiments to ensure that all samples can be studied appropriately.

The canola oil wax/hydrolyzate mixtures were heated up to and kept at 90 °C for 30 min to ensure complete dissolution of the waxes. Samples (400ml in a glass beaker, heating plate (MR Hei-Tech, Heidolph Instruments GmbH & Co.KG, Schwabach)) were agitated with a magnetic stirrer at 200 rpm. By careful pouring the solution into petri dishes samples of 40g (±1g) were prepared. The glassware was preheated (5 °C in excess of the targeted 90 °C to cater for initial cooling during the procedure) in order to prevent instantaneous crystallization on the container surface. To allow controlled sol–gel transitions the samples were stored for 48 h at 20.5 °C, temperature controlled within (±1.5 °C), prior to any analysis. To avoid any changes of the gels due to sample preparation the samples for calorimetrical, rheological and microscopical analysis were prepared directly out of the hot solution into the respective measurement environment.

2.2.2. Microscopy and Microstructural Analysis

Brightfield light microscopy (BFM) images were gathered with an Axio Scope.A1 KMAT (Zeiss, Jena Germany) equipped with an AxioCam ICm1 Rev.1 camera. Samples were prepared similarly to those in petri dishes. The slides were preheated to 95 °C before a drop of solution was administered. Once the cover glass was placed, the samples were kept at 20.5 °C for 48 h to undergo the sol–gel transition. Micrographs were taken without any further preparation.

The BFM-images were processed with ImageJ 1.52a. After the scaling and thresholding, the number and size of the crystals, number density, circularity and roundness were computed such that the BFM images also deliver quantitative information.

To reduce noise in the data, the circularity range considered was fixed to values between 0.1 and 1.0. The average sizes and number of detected crystals (count) were determined straightforwardly.

The number density describes the 2D coverage of the image surface by particle projections, expressed in %

$$\text{Number density} = \frac{\text{Total area of particles} \cdot 100}{\text{Total Area}} \tag{1}$$

Roundness characterizes the crystal shape as inverse aspect ratio (major axis/minor axis)

$$\text{Roundness} = 4 \cdot \frac{\text{Area of particles}}{\pi \cdot \text{major axis}^2} \tag{2}$$

Even though also the circularity approaches a value of 1 for a circular object it describes particles more defined by use of their perimeter

$$\text{Circularity} = 4\pi \cdot \frac{\text{Area of particles}}{\text{Perimeter}^2} \tag{3}$$

The fractal dimensions were determined by using the box counting method provided by Image J software. The box sizes were set to be 2, 3, 4, 6, 8, 12, 16, 32, and 64.

2.2.3. Cryo-SEM

Oleogel samples were cut in 1cm cubic pieces with a scalpel and successively immersed in 10ml isobutanol and ethanol for 24 h at 5 °C without stirring. After decanting the solvent, the samples were placed in a petri dish and dried under airflow. Next, the de-oiled sample was glued on a plane cryo transfer shuttle with conductive mounting medium (1:1 mix of Tissue-Tek O.C.T compound and colloidal graphite, Agar Scientific Ltd., Stansted, United Kingdom), plunge-frozen in nitrogen slush ($T = \approx -210$ °C) and transferred into the pre-cooled cryo chamber (PP2000 T, Quorum Technologies Ltd., Laughton, United Kingdom). Inside the cryo chamber the sample was sublimated at −90 °C for 15 min in order to remove possible residual ice contamination on the surface. To minimize charging problems, the

samples were sputtered with platinum in Argon atmosphere (30 s coating at ≈5–10 mA current) and finally transferred to the cryo stage in the SEM chamber ($T = -135$ °C). Imaging was carried out with a Quanta 250 FEG field emission scanning electron microscope (FEI, Brno, Czech Republic) under high vacuum conditions ($\sim 3 \cdot 10^{-7}$ mbar) with an Everhart-Thornley detector, a working distance of 5 mm and an accelerating voltage of 10 kV.

2.2.4. Calorimetry

Differential scanning calorimetry (DSC) was performed using a 214 Polyma (Netzsch, Selb, Germany) calorimeter. The sample size was 10mg (±1mg). The samples were also stabilized (48 h, 22 °C). Once in the DSC, the crucibles were cooled down to 5 °C without additional holding time to establish a stable baseline. Subsequently, the samples were heated from 5 to 105 °C with a heating rate of 5 °C min^{-1}. After a short holding time (2 min) a cooling scan from 105 to −10 °C with the same rate (5 °C min^{-1}) was performed.

2.2.5. Viscoelastic Behavior

The viscoelastic properties were analyzed with a MCR 302 rheometer (Anton Paar GmbH, Austria) using a parallel plate geometry. To avoid any slip a sandblasted PP25 ($d = 25$ mm) was used. To detect the sol–gel and gel-sol transitions both temperature and amplitude-strain-sweeps were performed. To distribute the samples on the geometry the hot liquid sample (approx. 5ml) was poured onto the preheated Peltier Plate ($T = 95$ °C). Final gap distance was 0.2 mm. For stabilization purposes the sample was kept for 10 min under shear ($\gamma = 1\ s^{-1}$). After 2 min under quiescent conditions, the samples were cooled down to 20 °C at a rate of 5 °C min^{-1}. During this scan, a constant strain of 0.1% and 10rad s^{-1} was applied. The gap distance was allowed to compensate sample contraction since the normal force was set to be zero.

Once the target temperature (20 °C) was reached, samples were isothermally stabilized under quiescent conditions for 15 min. Finally, the samples were subjected to a strain sweep ranging from 0.01–100% at an angular velocity of 10rad s^{-1}.

2.2.6. Firmness

The firmness measurements were performed with a zwickiLine universal testing machine from Zwick Roell (Ulm, Germany) equipped with a 1 kN load cell (trigger force 0.02 N). The samples in the petri dishes were penetrated for 30% of the sample height (2.9 mm ± 0.2 mm). The penetration speed was 200 mm min^{-1} and the probe head was a 12 mm diameter stainless steel cylinder. Each sample was characterized by 5 penetrations, at sufficient distance from each other. Values of maximum force were averages of 5 independent values though.

2.2.7. Statistical Analysis

One-way analysis of variance (ANOVA) was carried out with Origin Pro 9 (OriginLab, Northhampton, MA, USA) using a significance level of $p = 0.05$.

3. Results and Discussion

3.1. Microstructure

3.1.1. Light Microscopy

The BFM images for the different oleogels prepared are displayed in **Figure 1**. Samples were prepared as described above. All samples contain 8% (w/w) structurant. From left to right both waxes (SFW, BW) were stepwise substituted with the two hydrolyzates (SFWh, BWh). The left column shows pure unhydrolyzed wax samples.

The images indicate for SFW gels needle shaped structures. Careful assessment reveals that these structures are of "feathery" nature, thus most likely agglomerates of primary needle shaped crystals. This is in line with observations made previously.[4,27] H-S.Hwang, S. Kim, K. O. Evans, C. Koga, Y. Lee however, claimed these to be platelet-like crystals, orientated orthogonally to the cover of the microscope glass-slides.[28]

The beeswax-based samples (bottom left) show a different morphology revealing a more compact and irregular structure. Also, these crystals do appear to be agglomerates. Oleogels on basis of BW have been studied previously, e.g., by Jana and Martini[29] who found different morphologies in various oils. The interpretation of the BW crystal morphology is much less univocal than for SFW. The different results could be due to the sensitivity of BW to the crystallization process driven by its complex composition.[30]

As Figure 1 reveals, the partial replacement of SFW with hydrolyzates (SFWh, BWh) has a profound effect on the microstructure. A substitution with 25% BWh in the structuring system appears to only have a limited effect. The admixing of SFW-hydrolyzate (SFWh) in contrast changes the appearance significantly. On the other hand, the crystal agglomerates are apparently increasingly curved, thicker and feathered out. For 1:1 mixtures of the hydrolyzates with SFW this trend still persists. Once the hydrolyzed wax represents the major part (75:25), the morphology changes dramatically. For the BWh based system compact agglomerates with fewer junctions were found. This mixed structuring system behaves similarly to the pure BWh. For the SFW:SFWh mixture (25:75) the space filling structures are less well defined but maintain the feathery structure. Structuring with exclusively SFWh results in barely connected, isolated structures comparable to those found in the BWh system. In the series of mixture of BW and BWh it appears that with increasing BWh proportions, the structural elements become smaller and less clear identifiable by BFM. Once BWh becomes the prominent structurant, the agglomerates appear more prominently. As pointed out structuring with exclusively BWh yields distinct, compact, irregular agglomerates without indications for a space filling network. The stepwise substitution of SFWh for BW in this structuring system results in a similar evolution. Thus, initially a reduction of the crystal size, almost hazy samples without distinct crystal structures emerge. For higher levels of the SFW hydrolyzate the presence of compact agglomerates becomes more prominent.

Although one should be careful in overinterpreting the BFM images by taking the limitation to visualize smaller structural elements into account, clear effects of mixing could be identified.

European Journal of Lipid Science and Technology
www.ejlst.com

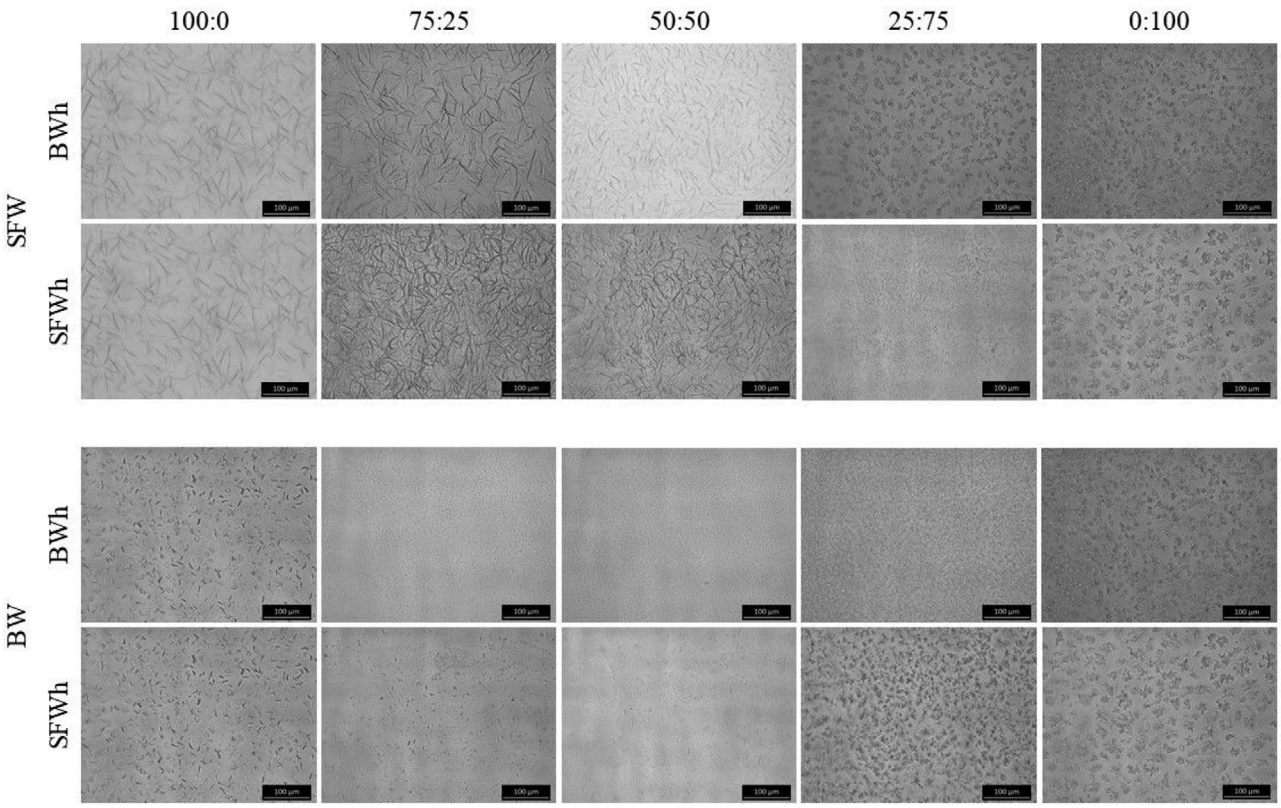

Figure 1. BFM images of 8 wt% oleogels with increasing amounts (left column to right column) of hydrolyzed wax. Scale bar indicates 100 µm. Pictures were taken at 200× magnification.

Microstructural Analysis: The characteristic data derived from the BFM micrographs are shown in **Figure 2**.

Microstructural features considered are average crystal, or agglomerate size, number of particles identified, number density (surface covered), box counting fractal dimensions, circularity and roundness. These data are primarily gathered to possibly unravel the link between microstructural characteristics and macroscopic properties such as firmness and rheological properties.[31–34] Overall, this approach is aiming to understand the relation between composition and macroscopic properties.

Confirming the visual impression of Figure 1, all characteristics derived vary greatly with changes of the composition of the structuring system. Independent of the structuring system concerned, reduced average crystal/aggregate sizes were found for the mixed structuring systems compared to "pure" waxes or "pure" hydrolyzates. This effect is more pronounced when wax and hydrolyzate origin from different sources. According to Figure 2, the elongated crystals/aggregates found in the SFW-based systems are by far the largest. Surprisingly, roundness and circularity show quite different trends. The relatively small variation of the roundness indicates limited changes in the habit. In contrast the significant changes in circularity on mixing structurants is possibly related to changes in the surface roughness of the agglomerates. Furthermore, the circularity evolves oppositely to the aggregate size. This is less pronounced for mixtures of SFW and SFWh. The data of number density and count derived for the SFW based system confirm the visual impression in Figure 1. However, the elongated aggregates identified for SFW:SFWh mixtures are sizable and cover a large fraction of the projection area (40%).

Plotting all data gathered according to the typical approach to characterize these types of systems via fractal dimension **Figure 3** emerges. Applying the box counting method[35] it is found that the fractal dimension D varies for the systems studied between 1.5 and 1.85 almost linearly with the number density. However, for a less densely covered BFM image (Number density = 8%) this correlation does not hold.

3.1.2. Cryo-SEM

As pointed out above, the observed structures in BFM vary greatly with different wax composition. It is notable at this point, that the size of the structures decreased when the amount of SFW was reduced and the resulting agglomerates became less needle-like shaped (Figure 1). Images from cryo-SEM are depicted in **Figure 4**.

According to the images, SFW forms relatively large, undefined, curved platelets that seem to aggregate to a porous 3-D structure. The image (upper left) suggests that the interwoven platelets themselves are aggregates of stacked crystals. Even though the images obtained by BFM and cryo-SEM are taken at different temperatures, they allow a consistent interpretation in line with H-S.Hwang, S. Kim, K. O. Evans, C. Koga, Y. Lee.[28]

European Journal of Lipid Science and Technology
www.ejlst.com

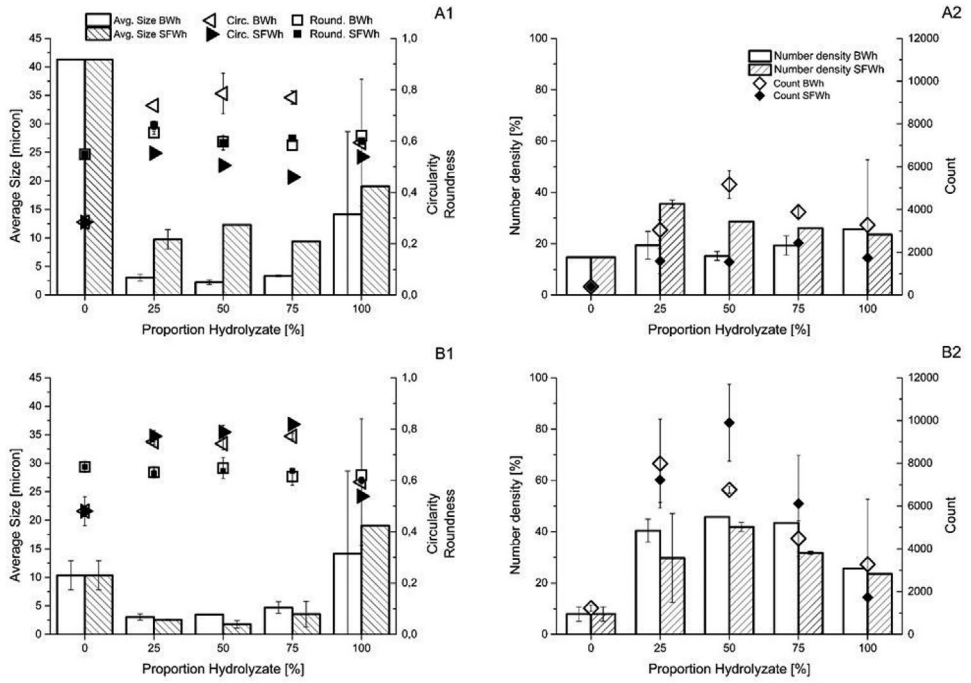

Figure 2. Microstructural characteristics derived from ($n = 2$) BFM images of 8 wt% oleogels. A1, A2) SFW:Hydrolyzate and B1,B2) BW:Hydrolyzates.

Taking the BFM-image as truly 2D cut in the focus area the cryo-SEM image supports the appearance of elongated, curved objects in the BFM images. Adding 50% hydrolyzate, whether BWh or SFWh, results in more curved but still platelet-like morphologies in the BFM images. However, the cryo-SEM images do not show such large objects (medium and bottom row, left columns). The structures formed show shortened plates with small pores. No visible differences can be distinguished between BWh and SFWh.

Likewise, BW shows smaller but also intertwined leaflet structures with small pore sizes. However, it can be seen that these also consist of platelet-like aggregates. As this observation is largely in agreement with the BFM images, the detected changes in BW:hydrolyzate 50:50 show practically no variation of the basic structures at 10 000-fold magnification (medium and bottom row, right columns). Mixing with 1 to 1 with SFW-hydrolyzate results in only minor changes in morphology as already indicated in BFM (Figure 1). It is surprising that the substitution of half the BW with either hydrolyzate does not yield structural changes that are detectable by BFM or cryo-SEM. The fact that the hardness values are highest for the mixtures (see 5.4) can possibly be explained by sequential crystallization of different molecular species.

However, for the BW-gels it is more difficult to derive a consistent structural interpretation that satisfies both, the BFM and cryo-SEM images for the compositions studied.

The images in the medium row of Figure 4 represent the same samples as in the bottom row. However, these reveal at half the magnification a very diverse topography of the samples, strongly depending on the position in the partially de-oilig cubic sample. The presence of areas quite different in appearance illustrate how prone to misinterpretations structure assessment by cryo-SEM remains.

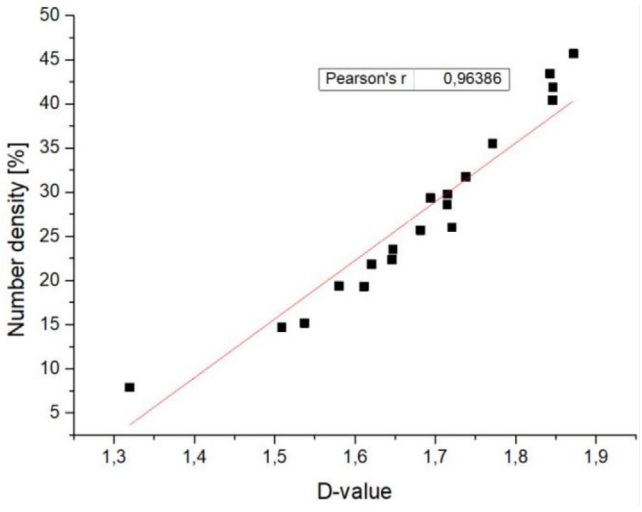

Figure 3. Plot of the overall mean values for the fractal dimensions D and number densities of 8% (w/w) oleogels.

3.2. Calorimetry

In **Figure 5** the set of thermograms gathered for the different systems are displayed. For the four systems heating (left) and cooling (right) thermograms of the wax and the 12% (w/w) gel are given. Only the thermograms relating to SFW as sole structurant show simple crystallization and melting behavior. In this case the high melting material is practically exclusively composed of wax esters, see composition in Table 2. Even

European Journal of Lipid Science and Technology
www.ejlst.com

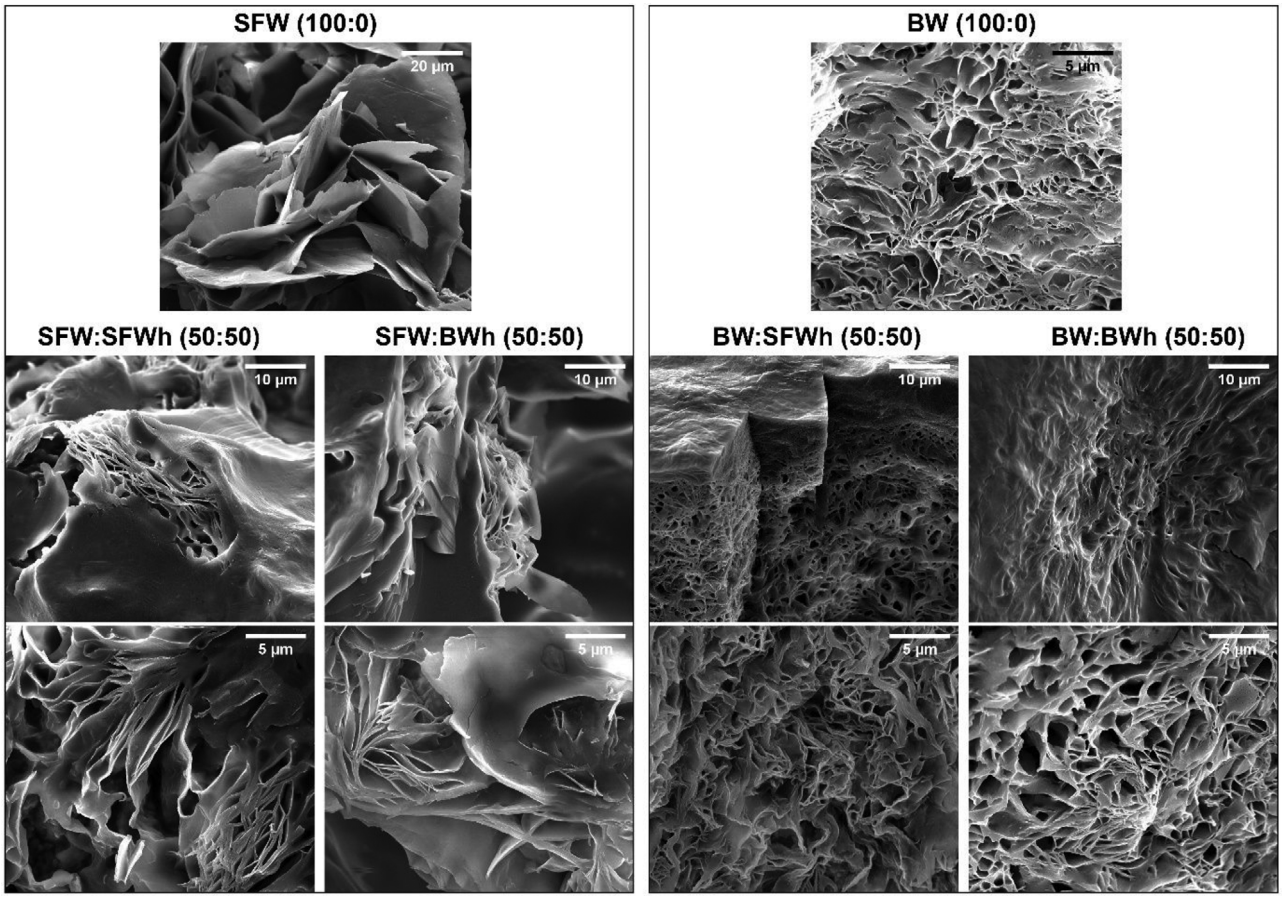

Figure 4. De-oiled cryo-SEM images of 10% (w/w) oleogels at different magnifications. From top to bottom: left image block 2500×, 5000×, 10 000×. Right image block 10 000×, 5000×, 10 000×. Scale bars are depicted in each image respectively.

though these wax esters cover a range of different combinations of fatty acids and fatty alcohols the thermograms suggest that a single solid phase, a solid solution, is present. For the other systems more complicated images emerge in DSC-scans. Multiple crystallization events appear on cooling of both the pure and the dilute systems. In the heating thermograms this behavior can be found back even though the signals of the lower melting or dissolving phases appear to be quite smeared out hampering a clear identification. The detailed interpretation of the thermograms needs to consider the different components or classes of components, wax esters, fatty acids, fatty alcohols and alkanes present in the samples. The respective profile of each sample with respect to these classes can straightforwardly be determined based on the information given in Table 2. In doing so, it is important to distinguish between the origin of the materials, since, e.g., the composition of fatty acid moieties in BW and SFW differ from each other. In the attempt to assign material to a specific peak, it is necessary to consider both material characteristics, melting temperature, heat of fusion, and the concentration in the sample. Even though data on different fatty acids and fatty alcohols are reported in literature,[23,24,36] it is difficult to derive these properties for the undefined mixtures present here. In any case, it seems justified to assume that the wax esters are related to the high temperature peaks as long as their concentration remains high. Considering the distinction between fatty alcohols and fatty acids the available data suggest that at equal chain length the fatty acids have a higher melting point temperature and a significantly higher heat of fusion. Following this reasoning, the DSC data were converted into solubility curves considering the different classes of material independently. This implies, the solute, either the mixture of or wax esters or fatty acids, or fatty alcohols is treated as a single pseudocomponent. This approach is basically in line with the lumping procedures applied in the modelling of reservoir fluids engineering.[37]

Figure 6a depicts the dissolution temperatures assigned to wax esters (WE) originating from SFW. The data originate from the systems SFW:SFWh, SFW:BWh and the respective gels with 12% structurant. Even though the accurate data extraction is complicated, see thermograms, the plotted data appear quite systematic. Open symbols represent composition of all wax esters while the grey symbols represent exclusively WE originating from SFW. The line drawn are based on the most simple approach to describe ideal solubilties,[38] see Equation (4). It has to be pointed out, that in this approach the liquid phase is treated as ideal solution.

$$x_i^L = \exp\left(-\frac{\Delta h_i^{FUS}}{R \cdot T} \cdot \left(1 - \frac{T}{T_i^{SL}}\right)\right) \quad (4)$$

European Journal of Lipid Science and Technology
www.ejlst.com

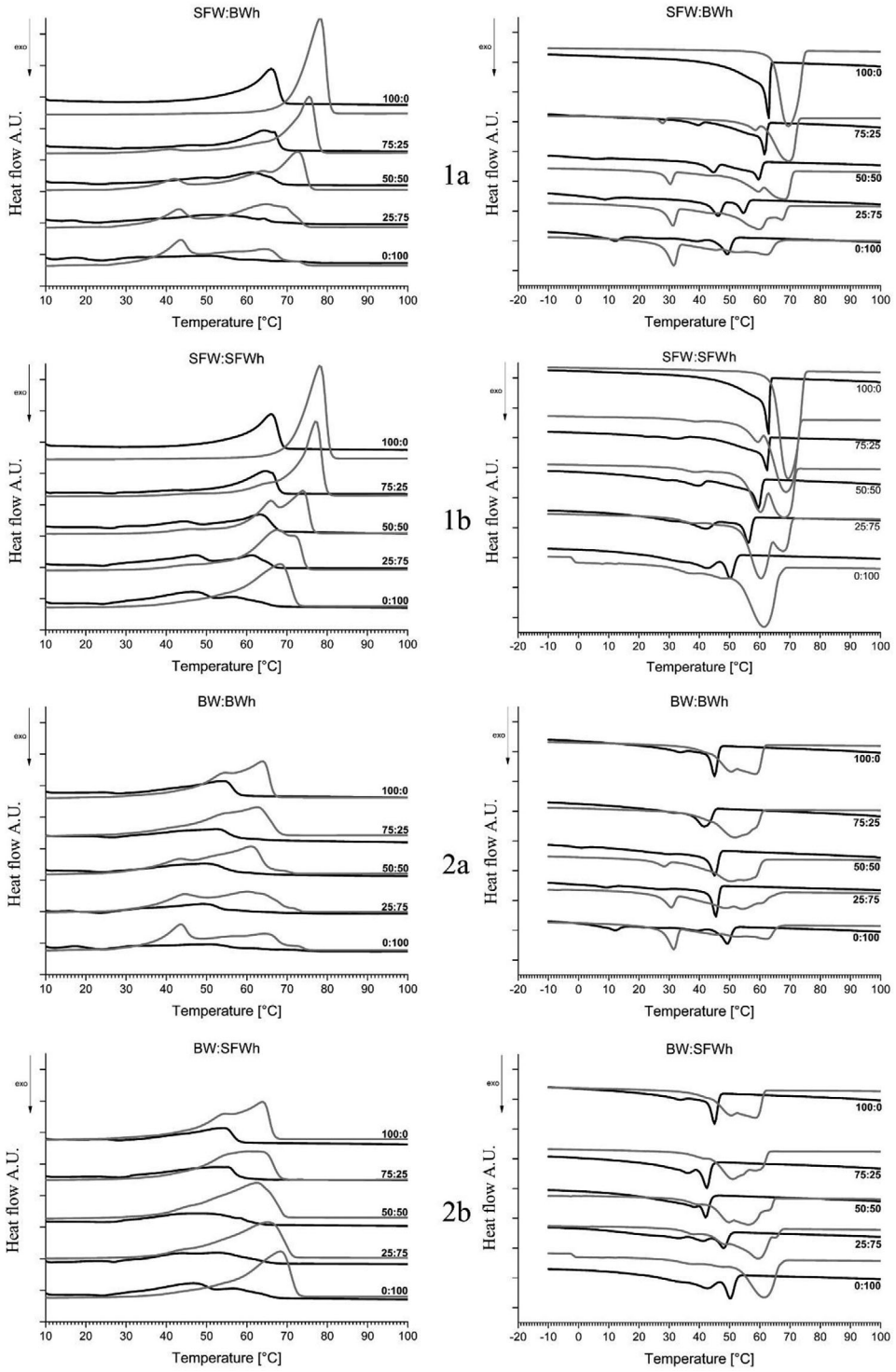

Figure 5. Mean thermograms(n = 3) of 12% (w/w) oleogels (black lines) and oil-free wax-mixtures (grey lines). Left: heating curves. Right: cooling curves. 1 = SFW, 2 = BW, a = BWh, b = SFWh.

Unfortunately, no characteristic data for the SFW wax esters is available. However, the data of Aydin et al.[39–41] on esters based on myristyl-, palmityl-, and stearyl-alcohol give helpful information. The data were used to develop a linear correlation of heat of fusion and carbon number for pure wax esters. This correlation is used to estimate the heat of fusion for the SFW wax esters. The mixture of wax esters in SFW is for this purpose represented by a single pseudocomponent wax ester with 47 carbons. This is the average of the reported, typical range.[26] This procedure resulted in an estimate of 176.6 kJ mol^{-1}. It is however known that

European Journal of Lipid Science and Technology
www.ejlst.com

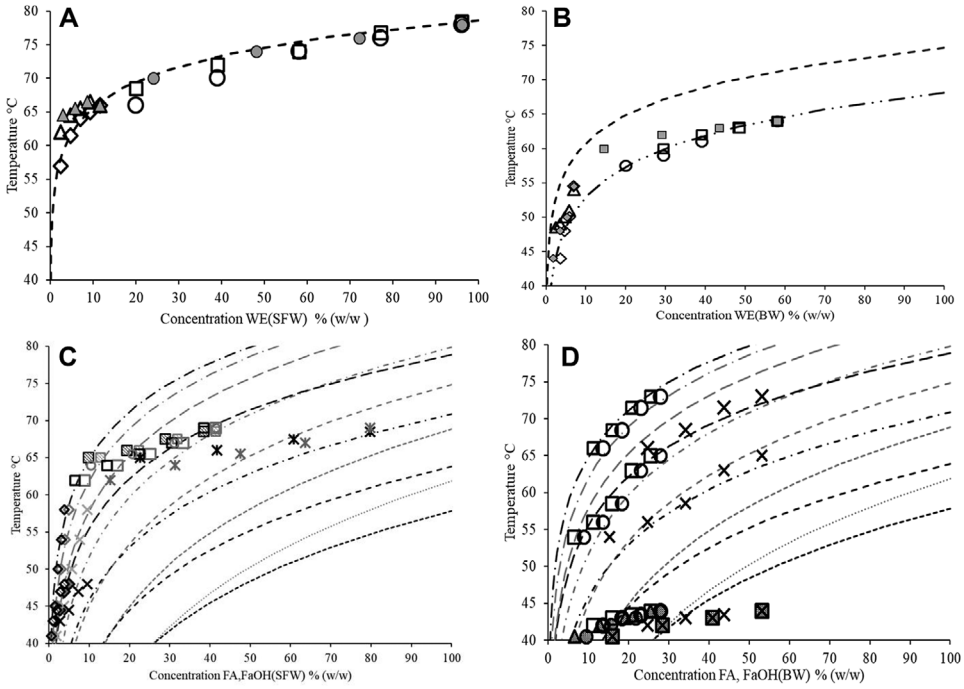

Figure 6. A) Solubility data and prediction for WE-pseudocomponent in SFW containing mixtures. Dashed line = prediction (Equation (4); T(SL) = 3518 K; dh = 1762 kJ mol^{-1}; both from correlations using average carbon number 47 for the pseudocomponent). All wax esters: squares (□) = WE SFW:SFWh (pure), Circles (○) = WE SFW:BWh (pure), Triangles (Δ) = WE SFW:BWh (oleogel) and diamond (◇) = WE SFW:SWh (oleogel). WE from SFW only: (○,grey) = WE SFW pure, Triangles (Δ,grey) = WE SFW oleogel. B) Solubility data and prediction for WE-pseudocomponent in BW containing mixtures. Dashed line = prediction (Equation (4); T(SL) = 3478 K; dh = 1606 kJ mol^{-1}; both from correlations using average carbon number 44 for the pseudocomponent), dashed-dotted line = fit (Equation (4); T(SL) = 3413 K; dh = 140 kJ mol^{-1}). Experimental data: All wax esters: (□) = WE BW:SFWh (pure), (○) = WE BW:BWh (pure), (Δ) = WE BW:BWh (oleogel), (◇) = WE BW:SWh (oleogel). WE from BW only: (□, grey) = pure, (◇,grey) = WE BW oleogel. C) Solubility data and prediction for fatty acids and fatty alcohols in SFW containing mixtures. Grey lines: solubility predictions (Equation (4) for FaOH's with increasing carbon numbers (18, 20, 22, 24, 26)), black lines: solubility predictions (Equation (4) for FA's with increasing carbon numbers (16, 18, 20, 22, 24, 26)). Both CN increasing from bottom up, physical properties melting point and heat of fusion extracted from NIST database/FaOH C24 and C26 derived by extrapolation. Experimental data: grey symbols: FA, black symbols: FaOH; (□, filled) = SFW:SFWh (pure), (□) = BW:SFWh (pure), (◇, filled) = SFW:SFWh (oleogel), (◇) = BW:SFWh (oleogel). Combined concentration FA+FaOH: (x, grey) = BW:SFWh (pure), (x, black) = SFW:SFWh (pure), (x, grey): BW:SFWh (oleogel), (x, black) = SFW:SFWh (oleogel)). (○) = FA only (BW:SFWh). D) Solubility data and prediction for fatty acids and fatty alcohols in SFW containing mixtures. Grey lines: solubility predictions (Equation (4) for FaOH's with increasing carbon numbers (18, 20, 22, 24, 26)), black lines: solubility predictions (Equation (4) for FA's with increasing carbon numbers (16, 18, 20, 22, 24, 26)). Both CN increasing from bottom up, physical properties melting point and heat of fusion extracted from NIST database/FaOH C24 and C26 derived by extrapolation. Experimental data: (□) = FaOH (pure), (○) = FA (pure), (x) = FA+FaOH (pure). Filled symbols = SFW:BWh (pure), open symbols = BW:BWh (pure). Data series of the same type are assigned to peaks occurring at different temperatures (*T*1 = 40–45 °C, *T*2 = 52–65 °C, *T*3 = 65–75 °C).

the melting point temperatures in a homologous series of chain molecules certainly do not scale with carbon numbers. Consequently, another approach to estimate the melting point was followed. The method outlined elsewhere (Seilert et al. to be submitted) yields an estimate of 351.8 K (78.65 °C). The predicted solubility curve computed based on these estimates and Equation (4) is shown. The evolution of the data and their description by the prediction given, suggest that the mixture of wax esters in the systems containing sunflower wax (SFW) behaves like a single component. This indicates that this wax ester phase itself is possibly best characterized as an ideal solid solution, which can be treated as a single pseudocomponent.

In Figure 6b, a similar picture as discussed previously emerges. The experimental data shown are related to peaks in the systems BW:SFWh, BW:BWh and their respective 12% gels. Again, the data extracted from the thermograms show a rather systematic pattern. The lines drawn are derived as described above, the dashed line represents a prediction of the solubility based on physical properties estimated according to the procedure outlined above. This yields an estimate for the enthalpy of fusion for the average carbon number of BW wax esters, $CN_{WE,\,BW}$ = 44, middle of the range from 40 to 48, equal to 160.6 kJ mol^{-1}. The estimated melting point temperature is 347.8 K (74.65 °C). The predicted solubility curve of this pseudo -wax ester systematically overpredicts the experimental solubility data. The dashed double dotted line is based on fitting the melting point temperature to the experimental data. The enthalpy of fusion to melting point temperature relation is maintaining as outlined by Seilert et al. The resulting properties for the pseudocomponent are melting point temperature 341.3 K (68.15 °C), heat of fusion 140 kJ mol^{-1}. Even though the melting point temperature had to be adjusted to describe the experimental data, the match found allows to draw a similar conclusion as for the SFW-wax esters. It appears justified to conclude that also the

wax esters of beeswax can with respect to solubility be treated as a single pseudocomponent. When the dissolution temperature data plotted against the concentration of the WE that originate exclusively from BW the deviation from the typical pattern increases. This supports the hypothesis that the WE from both sources can be considered to mix in the solid phase.

Other dissolution temperatures extracted from the thermograms cannot so easily be assigned to a specific component, or groups of components. Focusing on the fatty acids and fatty alcohols originating from SFW (SFW and SFWh), the temperatures determined are displayed versus the concentrations of either fatty acid (grey symbols (FA), black symbols (FaOH) or the combined concentrations of fatty acids and fatty alcohols (crosses). To also plot the data versus the concentration of the fatty alcohols is omitted for reasons of clarity. Regardless, this would result in minute shift of the data points concerning fatty acids to lower concentrations. In general, also these data appear quite systematic. Obviously displaying the temperature against FA (grey symbols) or FaOH (black symbols) deviates from using the combined concentrations (crosses). Additional to the experimental data, solubility curves calculated with Equation (4 are given. The characteristic properties used for the calculation are compiled from various sources (NIST database).[42] The different grey lines represent fatty acid solubility with increasing alkyl chain lengths (16 to 26 carbons, bottom to top). The black lines represent the calculated ideal solubilities for the series of fatty alcohols (C18 to C26, bottom to top). It has to be noted that the input data for C24 and C26 were derived by extrapolation of available data. Figure 6c reveals that the solubility curves of neither fatty acids nor fatty alcohols represent the experimental dissolution data over the whole composition range studied. Solubility curves computed for either pure C24 fatty alcohol or C22 fatty acids approximate the experimental data in the composition range below 10%. The comparison of experimental data under the assumption that solid phases present can be described as either ideally mixed FA, FaOH or a solid mixture does not allow to draw any conclusion with respect to assigning component to specific events. However, defining a pseudocomponent with a melting temperature of 344 K (70.85 °C) and a heat of fusion of 160 kJ mol^{-1} allows to describe the data of temperature versus combined concentration fairly well (data not shown). This might be taken as a token for the formation of solid phases composed of fatty acids and fatty alcohols.

Figure 6d is concerned with the data relating to fatty acids and/or fatty alcohols originating from the beeswax (BW and BWh). Again, the temperatures (*T* high and *T* low) are plotted versus the concentrations of the individual pseudocomponents or the cumulated concentration – fatty acids: circles; fatty alcohols: squares; sum: crosses. In contrast to the other data sets it is striking that the dissolution temperature determined seems to depend significantly on the non-hydrolyzed wax the BWh is mixed with. For mixtures with basically the same composition with respect to fatty acids and fatty alcohols, originating from BWh, the dissolution temperatures found in combinations with SFW is up to 10 °C higher than those in combinations with BW. As stated above, the main fatty acid in beeswax is palmitic acid (C16). In contrast to expectation that experimental data are close to calculated C16 FA solubility, good matches are obtained for either long chain fatty acids or long chain fatty alcohols (C24OH: BW/BWh; C26OH: SFW/BWh). When plotting the temperatures derived from the thermograms against the combined concentrations of fatty acids and fatty alcohols, the evolution of the data points is also reasonably well approximated by the solubility curves predicted. Rather speculative, seen the very limited data available on the mixing behavior of these components (FA, FaOH), this could be an indication for fatty acid-fatty alcohol mixed crystal formation at high temperatures (BWh/SFW and BWh/BW). The peaks identified at lower temperatures also show a systematic behavior. The evolution of the experimental values, however, does not correspond to any solubility prediction of the relevant materials. In any case, these crystallization events can certainly not be assigned to the wax esters. However, it should be noted that the dissolution data considered, concern temperatures clearly lower than any melting point temperatures. It is worthwhile to consider the complicated phase diagrams of mixed *n*-alkanes of similar chain length, that show enantiotropic polymorphism,[38] in case more stable low temperature polymorphs are in equilibrium with the solution, next to the heat of fusion also the heat of transition has to be taken into account when computing solubilities. This could result in quite different characteristics, dissolution temperature and heat of fusion, for mixed solid phases.

The DSC thermograms of the different mixtures of waxes and wax hydrolyzates offer an insight into the complicated crystallization behavior of mixtures containing at least three types of molecules, wax esters, fatty acids and fatty alcohols. Due to presence of beeswax, additionally a fraction of alkanes is introduced to the mix. On top, the variation within each fraction cannot be neglected. It is found that the data gathered are, in particular considering the fact that a specific type of wax is rather ill defined, in good agreement with literature data.[16,27] By disentanglement of the peak temperatures and their assignment to material classes it was found that the solubility of the wax esters can be described quite well by computing ideal solubilities based on the assumption that the wax ester phase behaves like a single pseudocomponent. This indicates that the interaction between the wax esters and the other components in the mix are negligible. Regarding fatty acids and fatty alcohols, a more complex situation was found. Even though the data are found to be quite systematic, their consistent description with simple solubility predictions is less successful. Individual data sets are reasonably described by assigning mainly long chain fatty alcohols, see Figure 6d. A comprehensive interpretation is only obtained when considering that fatty acids and fatty alcohols form mixed solid phases. This assumption is in line with findings on synergistic effects reported by M. Callau, K. Sow-Kébé, L. Nicolas-Morgantini, A.-L. Fameau[23] on mixtures of behenic acid and behenyl alcohol and F. G. Gandolfo, A. Bot, Eckhard Flöter[22] on the mixtures of fatty acids and fatty alcohols.

3.3. Viscoelastic Behavior

The formation of oleogels was studied rheologically. The left column of **Figure 7** shows temperature sweeps (TS) for different structuring systems investigated at a 12% (w/w) concentration. The two top samples illustrate the effect of hydrolyzate substitution for SFW (a: BWh; b: SFWh). Applying 12% SFW results in a clear crystallization event at 63.96 °C (±1.32 °C) with the respective modulus change. Changing the composition of the

European Journal of Lipid Science and Technology
www.ejlst.com

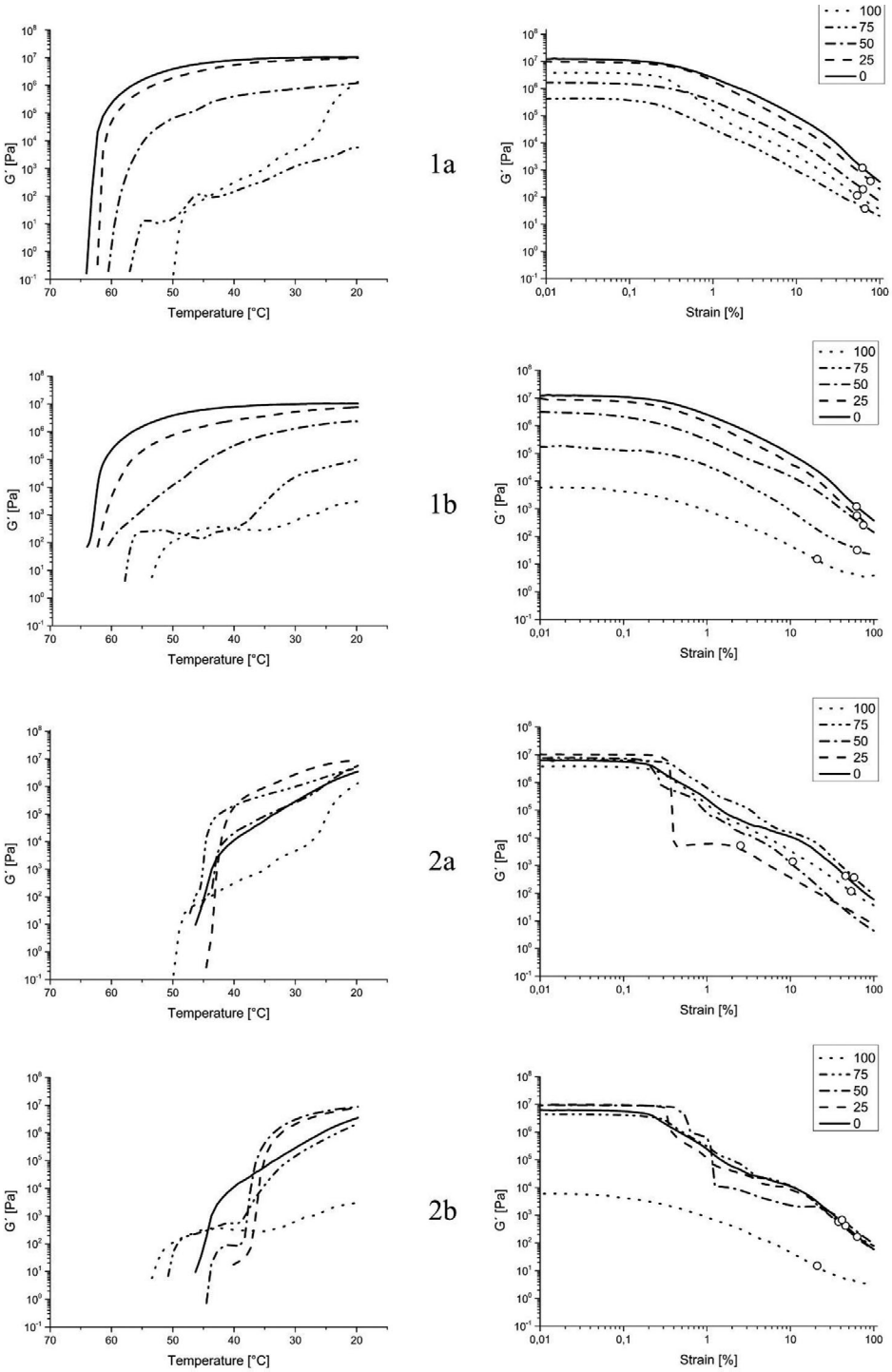

Figure 7. Temperature sweeps (left column) and Amplitude strain sweeps (right column) for 12 wt% wax oleogels, where 1 = SFW, 2 = BW, a = BWh, b = SFWh. For better overview, only elastic moduli are presented. Circles (o) indicate yielding point (G' = G''). Solid lines present neat waxes (SFW or BW). Dotted line shows 100% hydrolyzate in corresponding mixtures.

structuring systems to 25% BWh and 75% SFW results only in a shift to slightly lower temperatures with the moduli at lower temperatures practically unchanged. For a 50% (w/w) mixture of SFW and BWh G'- values of 1.05E+07 Pa at low temperatures drop by one decade. On further substitution of BWh for SFW the sol–gel transition temperature further decreases. After an initial steep rise in elastic modulus the curves show a continuous but much flatter increase of G' on temperature reduction. Surprisingly, the mixture of 25% SFW and 75% BWh shows an additional step in elastic modulus at approximately 25 °C,

European Journal of Lipid Science and Technology
www.ejlst.com

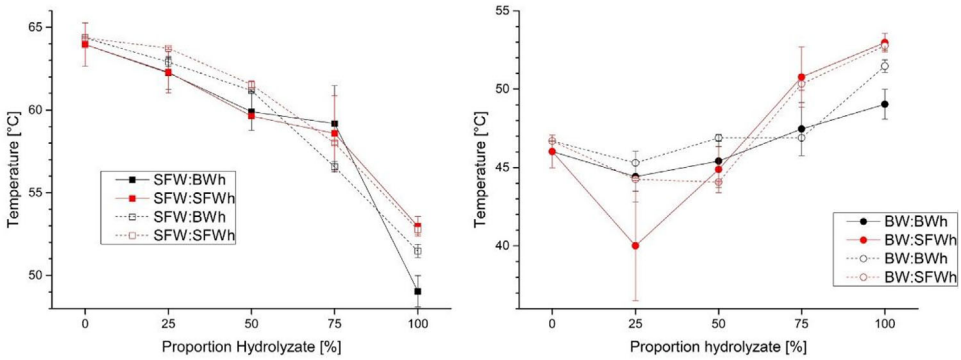

Figure 8. Comparison of thermal (DSC, cooling) and elastic response of 12 wt% oleogels (5 °C min^{-1}). Filled symbols show data from TS (sol–gel transition) and hollow symbols data from DSC (onset crystallization). Tsol–gel and Tonset are connected by lines for each mixture.

indicating an additional crystallization event. When instead of BWh, SFWh is used in combination with SFW, a very similar picture emerges. For the mixtures with up to 50% of hydrolyzate the effect of substitution is more pronounced. However, for both mixtures predominantly containing SFWh the initial steep increase of the elastic modulus is followed by plateauing with constant moduli for a temperature range of approximately 20 °C (see 1b). At temperatures below 40 °C a slow further increase of the moduli was detected.

For the structuring systems based on BW a more complicated picture emerges. As also seen in the DSC results, the pattern of crystallization events is quite different for BW based systems compared to SFW which is predominantly composed of WE. The substitution by hydrolyzates causes an onset reduction in SFW system and in the BW system an increase. For mixtures containing BW, the development of the elastic modulus with decreasing temperature is less smooth than in the SFW systems. This indicates possible multiple sequential crystallization events, relating to wax esters, fatty acids and fatty alcohols. In comparison of the two BW-based systems, it is striking that the distinction of separate crystallization events is much clearer in the system containing SFWh. Regarding the elastic moduli observed at the end of the temperature sweep (20 °C), all BW samples containing BWh approach similar values. The effect of substituting hydrolyzate for untreated wax is much less pronounced in the BW based systems. This is particularly true for the systems containing 75% hydrolyzates.

In an attempt to relate the differences in crystallization found to the characteristics of the raw materials it is necessary to take a detailed look at the composition of the different materials present. It remains undisclosed what material (WE, FA FaOH) crystallizes at the highest temperatures in the BW-based samples. If it is assumed that these are wax esters, one would assign the second crystallization to either fatty acids or fatty alcohols. Only considering fatty acids, predominantly C16, BWh containing should crystallize at lower temperatures than those originating from SFWh, mainly C20. The data in contrast indicate the opposite. This, considering Figure 6d supports that long-chain fatty alcohols play a role in this second crystallization event. Alternatively, assuming a different sequence assigning the first crystallization incident to the fatty acids present the interpretation does not become any better. In case the second step is related to wax esters the ones originating from SFW (2b) would also crystallize at higher temperatures than those of BW (2a). Similarly, to the analysis of the DSC data, this suggests that in particular in the systems containing beeswax the different classes of molecules do not crystallize independently from each other. To unravel this is clearly beyond the scope of the work reported here. The knowledge of the complex interaction between fatty acids and fatty alcohols[22–25] indicates that the complex interaction of the alkyl moieties present deserves further attention.

To further justify the utilization of the DSC results in the interpretation of the rheological results the temperatures of crystallization events and offsets for moduli increase were compared. To this end the onset of the DSC peaks in the cooling curves were considered (Figure 5, right column). For obvious reasons only samples composed of 12% (w/w) are shown. **Figure 8** shows the temperatures determined for the first crystallization event for all four systems. Taking into account that crystallization under shear (oscillation), mild though, and under quiescent conditions (DSC) are compared, the agreement between the data is quite good. The fact that counterintuitively the temperatures derived from rheology are lower than the DSC-based data, possibly relates to the fact that initial crystallization is not necessarily equivalent to the appearance of a space filling network, which is detected. The data further indicate that there is no structural difference with respect to mixed crystal formation between oscillating shear and quiescent conditions.

The right column of Figure 7 shows the data obtained by amplitude strain-sweeps subsequent to 15 min isothermal rest of the samples at 20 °C. In broad terms all four samples show a similar behavior: continuous reduction of the elastic modulus on strains greater than 0.2%.

The fact that the start values of these measurements are elevated compared to those obtained at the end of the temperature sweep is not surprising. This is line with I. Tavernier, C. D. Doan, D. van de Walle,S. Danthine, T. Rimaux, K. Dewettinck, reporting that wax gels tend to post-crystallize and hence post-harden.[11] This effect is most accentuated in the sample containing 25% SFW and 75% BWh. Most prominent difference between the samples are the discontinuities in the BW-based samples. These corresponds well with the multiple crystallization events on cooling. Even though this effect is less clear throughout the set of samples, it is an indication that these gels are sensitive to shear

European Journal of Lipid Science and Technology
www.ejlst.com

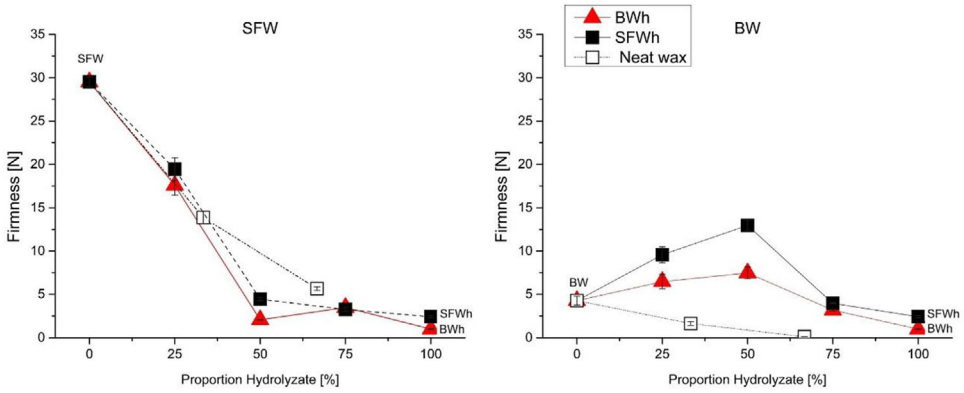

Figure 9. Mean Fmax-values of 12 wt% wax-oleogels ($n = 5$) with increasing proportions of hydrolyzate. Dash, double dotted lines show theoretical contribution (based on lower wt% measurements) of neat BW and SFW to firmness values.

and deformation ($\gamma \approx 0.4\%$). The gel-sol transition points determined, indicated as circles, appear to be rather uncharacteristic.

3.4. Firmness

In **Figure 9**, the firmness of 12 wt% oleogels based either on SFW (left) or BW (right) are shown. The firmness of the different samples was assessed as described above. This means that the samples studied here were stored isothermally for 48 h prior to analysis.

As already identified in the rheological measurements, the sample containing exclusively SFW is the hardest. The data on SFW-based samples indicate that the structure is almost exclusively due to wax ester crystals. The decline of the hardness practically scales with the SFW-concentration up to 50% substitution. At higher inclusion levels of the hydrolyzates hardness varies around lower values. The same trend can also be found in the circularity data, Figure 2. Counterintuitively, the reduced aggregate size and higher crystal count seems to have a less pronounced effect on gel strength in SFW mixtures. This might however be due to the resolution of the BFM. It is furthermore noteworthy that the relative hardness of these samples does not correspond to the data gathered by rheological measurements. In these measurements the samples with 75% hydrolyzate were particularly soft. These differences are possibly an indication for the effect of shear on structure formation. For gels based on BW and its mixtures macroscopic hardness and rheological assessment are in much better agreement. The data displayed in Figure 7 indicate that for the SFW-based samples crystallization is practically completed long before the resting period to stabilize the samples at 20 °C starts. In contrast, the BW-samples appear to still be crystallizing at this state of the procedure. Even though this needs further confirmation, this suggests that the kinetics of the crystallization compared to duration of the measurement, thus partial crystallization under quiescent conditions, are key to these differences.

The earlier identified sintering effect due to stepwise crystallization in the intermediate composition range is confirmed by maximum hardness values for 50% mixtures of BW and hydrolyzates, Figure 9 right. The difference found between the oleogels containing SFWh and BWh is not fully in line with the with results shown in Figure 7. As described above this could be due to the timescales of crystallization and shear in the rheometer because sintering typically occurs once secondary crystallization occurs under quiescent conditions.

4. Conclusion

The work presented is concerned with the need to understand the contribution of different molecular species in different waxes to the oil structuring functionality. Even though the detailed analysis of different waxes is scarce, it is important to understand the individual contribution of wax esters, fatty acids and fatty alcohols. In order to facilitate the change from working with raw materials to working with molecular compositions, oleogels based on waxes and hydrolyzates were studied. Four structuring systems each composed of either bees or sunflower wax and a wax hydrolyzate were studied. This allowed to systematically vary the relative concentration of wax esters versus fatty acids/fatty alcohols. When mixing materials from the same origin the overall fatty acid/fatty alcohol composition, either free or ester bound, remained unchanged. In the other systems mixing also resulted in the variation of the mix of alkyl chain moieties.

Optical assessment by brightfield light microscopy and cryo-SEM did not allow to draw a convincing structural hypothesis. Still, the combined data suggest that SFW develops a continuous structure of relatively large leaflets. In BFM these appear due to the 2D of the focal area as curved needles. It is found that the macroscopic properties do not match with the typical reasoning considering the observed morphologies. Assuming comparable particle-particle interaction it is fair to claim that smaller structural elements result in stronger structures. That the rather coarse structure found in SFW gels results in the hardest gels proves this line of reasoning wrong and deserves further investigations. Surprisingly structural efficiency in the SFW-based gels is not improved by addition of low-melting components which are supposed to result in excess hardness due to sintering. This effect is found in mixtures containing BW where maximum hardness values were observed at intermediate mixing ratios.

The detailed analysis of the data gathered by DSC and rheology allow to disentangle the crystallization of different classes of materials. Surprisingly, the solubility of the wax esters phase

can be described by ideal solubility calculations assuming a single "wax ester pseudocomponent." The description of the behavior of the fatty acid and fatty alcohol fractions appears more complicated. In line with earlier findings on co-crystallization of specific pairs of these components it is likely that depending on the sample composition and the respective chain length make up fatty acids and fatty alcohols do form mixed crystals or crystallize separately. The DSC and rheological data further suggest that sequential crystallization events occur depending on the molecular composition of the samples. Despite, the very consistent indication – small structural elements, high melting points, sequential crystallization and structural properties derived from the rheological measurements – suggesting that BW and BWh are good structurants, the SFW clearly delivers the highest macroscopic hardness. In this assessment (penetrometry) the hardness of the SFW samples scales with the inclusion level of the SFW. For the BW-based samples the described effect of sequential crystallization with increased hardness is also manifested at the macroscopic level as intermediate compositions result in highest hardness. In summary the data gathered and the data processing performed mark an initial step towards the unravelling of the different molecular fractions in waxes with respect to their functionality in oleogelation.

Supporting Information

Supporting Information is available from the Wiley Online Library or from the author.

Acknowledgements

This research has been funded by cooperative industrial research of the German federation of industrial research associations (AiF) and cooperative industrial research (FEI) (AiF 20285 N). Special thanks go to Karl Peleikis (Kahlwax GmbH) who provided helpful information. For the persistent support and precise work, the authors would like to thank Vivien Schreiber (TU Berlin). The authors would also like to thank Olaf Baumgart (Gustav Heess GmbH) for his willing support and Simone Brümmer for excellent technical support with the cryo-SEM analyzes.

Conflict of Interest

The authors declare no conflict of interest.

Keywords

fatty acids, fatty alcohols, oleogels, waxes, wax esters

Received: November 9, 2020
Revised: April 22, 2021
Published online: June 12, 2021

[1] N. M. de Roos, M. L. Bots, M. B. Katan, *Arterioscler., Thromb., Vasc. Biol.* **2001**, *21*, 1233.
[2] P. Wassell, N. W. G. Young, *Int. J. Food Sci. Technol.* **2007**, *42*, 503.
[3] M. A. Rogers, *Food Res. Int.* **2009**, *42*, 747.
[4] A. I. Blake, A. G. Marangoni, *Food Biophys.* **2015**, *10*, 403.
[5] H. S. Hwang, M. Singh, J. K. Winkler-Moser, E. L. Bakota, S. X. Liu, *J. Food Sci.* **2014**, *79*, C1926.
[6] M. Scharfe, E. Flöter, *Eur. J. Lipid Sci. Technol.* **2020**, *12*, 2000213.
[7] H.-S. Hwang, J. D. Gillman, J. K. Winkler-Moser, S. Kim, M. Singh, J. A. Byars, R. L. Evangelista, *J. Am. Oil Chem. Soc.* **2018**, *95*, 557.
[8] S. Jana, S. Martini, *Food Res. Int.* **2016**, *89*, 245.
[9] L. S. K. Dassanayake, D. R. Kodali, S. Ueno, K. Sato, *J. Am. Oil Chem. Soc.* **2009**, *86*, 1163.
[10] L. S. K. Dassanayake, D. R. Kodali, S. Ueno, K. Sato, *J. Oleo Sci.* **2012**, *2012*, 1.
[11] I. Tavernier, C. D. Doan, D. van de Walle, S. Danthine, T. Rimaux, K. Dewettinck, *RSC Adv.* **2017**, *7*, 12113.
[12] J. A. Morales-Rueda, E. Dibildox-Alvarado, M. A. Charó-Alonso, R. G. Weiss, J. F. Toro-Vazquez, *Eur. J. Lipid Sci. Technol.* **2009**, *111*, 207.
[13] A. Jang, W. Bae, H.-S. Hwang, H. G. Lee, S. Lee, *Food Chem.* **2015**, *187*, 525.
[14] J. Lim, S. Jeong, K. Im Oh, S. Lee, *LWT* **2017**, *84*, 788.
[15] B. Yi, M.-J. Kim, S. Y. Lee, J. Lee, *Food Sci. Biotechnol.* **2017**, *26*, 79.
[16] J. K. Winkler-Moser, J. Anderson, F. C. Felker, H.-S. Hwang, *J. Am. Oil Chem. Soc.* **2019**, *96*, 1125.
[17] M. Scharfe, Y. Ahmane, J. Seilert, J. Keim, E. Flöter, *Eur. J. Lipid Sci. Technol.* **2019**, *121*, 1800487.
[18] C. D. Doan, I. Tavernier, P. K. Okuro, K. Dewettinck, *Innovative Food Sci. Emerging Technol.* **2018**, *45*, 42.
[19] A. I. Blake, A. G. Marangoni, *Food Biophys.* **2015**, *10*, 456.
[20] E. J. Pérez-Monterroza, C. J. Márquez-Cardozo, H. J. Ciro-Velásquez, *LWT–Food Sci. Technol.* **2014**, *59*, 673.
[21] M. Chopin-Doroteo, J. A. Morales-Rueda, E. Dibildox-Alvarado, M. A. Charó-Alonso, A. La Peña-Gil, J. F. Toro-Vazquez, *Food Biophys.* **2011**, *6*, 359.
[22] F. G. Gandolfo, A. Bot, E. Flöter, *J. Am. Oil Chem. Soc.* **2004**, *2004*, 1.
[23] M. Callau, K. Sow-Kébé, L. Nicolas-Morgantini, A.-L. Fameau, *J. Colloid Interface Sci.* **2019**, *560*, 874.
[24] C. Blach, A. J. Gravelle, F. Peyronel, J. Weiss, S. Barbut, A. G. Marangoni, *RSC Adv.* **2016**, *2016*, 81151.
[25] H. M. Schaink, K. F. van Malssen, S. Morgado-Alves, D. Kalnin, E. van der Linden, *Food Res. Int.* **2007**, *40*, 1185.
[26] C. D. Doan, C. M. To, M. d. Vrieze, F. Lynen, S. Danthine, A. Brown, K. Dewettinck, A. R. Patel, *Food Chem.* **2017**, *214*, 717.
[27] C. D. Doan, I. Tavernier, M. D. B. Sintang, S. Danthine, D. van de Walle, T. Rimaux, K. Dewettinck, *Food Biophys.* **2017**, *12*, 97.
[28] H.-S. Hwang, S. Kim, K. O. Evans, C. Koga, Y. Lee, *Food Struct.* **2015**, *5*, 10.
[29] S. Jana, S. Martini, *J. Agric. Food Chem.* **2014**, *62*, 10192.
[30] S. Jana, S. Martini, *J. Am. Oil Chem. Soc.* **2016**, *93*, 543.
[31] T. Imai, K. Nakamura, M. Shibata, *Colloids Surf. A.* **2001**, *194*, 233.
[32] S. Yuping, L. Baomin, W. H. Richard, *J. Am. Oil Chem. Soc.* **2005**, *2005*, 399.
[33] S. S. Narine, A. G. Marangoni, *Phys. Rev. E* **1999**, *59*, 1908.
[34] Y. Miyazaki, A. G. Marangoni, *Mater. Res. Express* **2014**, *1*, 25101.
[35] T. G. Smith, G. D. Lange, W. B. Marks, *J. Neurosci. Methods.* **1996**, *69*, 123.
[36] J. A. Wilson, J. S. Chickos, *J. Chem. Eng. Data* **2013**, *58*, 322.
[37] H. Alkandari, A. Elsharkawy, A. Malallah, O. Alomair, *J. Eng. Res.* **2018**, *5*, 1.
[38] *Crystallization of Lipids: Molecular Interactions and Mixing Phase Behavior of Lipid Crystals* (Ed: K. Sato), John Wiley & Sons Ltd, West Sussex, UK **2018**.
[39] A. A. Aydin, A. Aydin, *Sol. Energy Mater. Sol. Cells* **2012**, *2011*, 93.
[40] A. A. Aydin, *Sol. Energy Mater. Sol. Cells* **2011**, *2013*, 77.
[41] A. A. Aydin, O. Hasancan, *Sol. Energy Mater. Sol. Cells* **2011**, *2011*, 2752.
[42] F. Valoppi, S. Calligaris, A. G. Marangoni, *Eur. J. Lipid Sci. Technol.* **2017**, *119*, 1600252.

